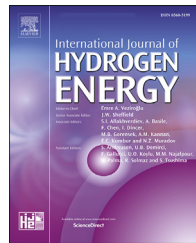




ELSEVIER

Available online at www.sciencedirect.com**ScienceDirect**journal homepage: www.elsevier.com/locate/he

K and halogen binary-doped graphitic carbon nitride ($\text{g-C}_3\text{N}_4$) toward enhanced visible light hydrogen evolution

Qiu-Hui Zhu ^{a,b}, Zhou Chen ^{a,***}, Li-Na Tang ^{a,b}, Yue Zhong ^{a,b},
Xiu-Feng Zhao ^b, Li-Zhong Zhang ^{b,**}, Jian-Hui Li ^{a,*}

^a National Engineering Laboratory for Green Chemical Productions of Alcohols, Ethers and Esters, College of Chemistry and Chemical Engineering, Xiamen University, Xiamen 361005, PR China

^b Department of Chemistry and Applied Chemistry, Changji University, Changji 831100, PR China

HIGHLIGHTS

- We systematically studied the effect of K and halogen binary-doped graphitic carbon nitride on photocatalytic performance.
- The significantly enhanced photocatalytic activity is described to the double accelerations of F, K binary doping.
- F–K–C₃N₄ exhibits improved visible light harvesting ability and photogenerated charge separation rate.
- The F–K–C₃N₄ exhibits 8.5 times higher H₂ generation rate than that of pristine C₃N₄.

ARTICLE INFO

Article history:

Received 5 July 2019

Received in revised form

29 August 2019

Accepted 1 September 2019

Available online 24 September 2019

Keywords:

Photocatalysis

Carbon nitride

K, F co-doping

Visible light

Solar energy

ABSTRACT

Water splitting driven by solar energy to produce hydrogen, which is highly dependent on the designing of semiconductor photocatalyst, is an efficient technology to address energy shortage problems and environment issues simultaneously. Here, the halogen and potassium binary-doped graphitic carbon nitride (named as X-K-C₃N₄, X = F, Cl, Br, I) photocatalysts were synthesized via simply one pot thermal polymerization method, which shown optimized band structure, enhanced optical absorption, higher separation rate of photogenerated carriers, and thus improved photocatalytic performance under visible light irradiation. As result, F–K–C₃N₄ is demonstrated to be highly efficient in the separation and transfer of carriers owing to the existence of C–F bond, C≡N triple bond and K junction. The F–K–C₃N₄ shows a highest H₂ evolution rate of 1039 μmol g⁻¹ h⁻¹ and a remarkable stability under visible light irradiation ($\lambda \geq 420$ nm), which is about 8.5 times higher than that of pristine g-C₃N₄.

© 2019 Hydrogen Energy Publications LLC. Published by Elsevier Ltd. All rights reserved.

* Corresponding author.

** Corresponding author.

*** Corresponding author.

E-mail addresses: 20520160154064@stu.xmu.edu.cn (Z. Chen), zhanglz12345@sina.com (L.-Z. Zhang), jhli@xmu.edu.cn (J.-H. Li).

<https://doi.org/10.1016/j.ijhydene.2019.09.013>

0360-3199/© 2019 Hydrogen Energy Publications LLC. Published by Elsevier Ltd. All rights reserved.

Introduction

Currently, the energy crises become one of the most challengeable issues with the rapid development of modern industrialization, which is seriously impeding the progress and development of human society [1–4]. Since the pioneering study guided by Fujishima and Honda in which photo-assisted electrochemical decomposition of water was triumphant carried by TiO₂ catalyst in 1972 [5], solar-driven energy utilization and conversion has become one of the most promising research fields. It is important to note that the photocatalytic H₂ evolution shows great potential for alleviating energy crises, in which photocatalyst play an indispensable role in converting solar energy into chemical energy [6–13]. However, the low optical quantum conversion efficiency of photocatalyst greatly restricts the efficient utilization of solar energy. Therefore, exploring effective photocatalyst with high light quantum efficiency under visible light irradiation has focused many attentions to realize the practical application of photocatalysis [14–17].

In recent years, a polymer semiconductor, namely graphitic carbon nitride (g-C₃N₄), consists of heptazine units formed through sp² hybridization of carbon and nitrogen alternately, plays an increasingly significant role in photocatalytic field [18]. The unique structure endows it with many advantages such as high physicochemical stability, unique band gap configuration (2.7 eV), which has attached growing attention in visible light photocatalytic solar-to-H₂ conversion system [19]. Previous reports determined that the conduction band, constituted by C 2p orbital, is located at -1.3 V (vs. NHE) and the valence band, constituted by N 2p orbital, is located at 1.4 V (vs. NHE), which is competent to the theoretical calculation of photocatalytic water splitting [20–23]. However, facing some intrinsic drawbacks such as unsatisfactory visible light absorption ability, rapid recombination of photoinduced electron-hole pair sharply restricts its practical application [24,25].

In fact, extensive studies have been carried to explore facile and dependable strategies to improve the photocatalytic efficiency of g-C₃N₄ based photocatalysts under visible light, for examples, introduction of heteroatoms [7,26,27], interaction with conductive metals [28] and nonmetals [29], coupling with other semiconductor materials [30], or activation by organic dyes [31]. Among these approaches, heteroatom doping is an efficiently and broadly proposed route to promote the visible-light responsive semiconductor photocatalysts [32–34]. To date, the most common approaches to elevate g-C₃N₄ photocatalytic activity include B, C, S, O, K and halogen elements. Several studies have demonstrated that oxygen doping could enhance absorption ability and modify electronic properties and charge transport, resulting in improved utilization of visible light and separation rate of electron and hole pairs [35]. In addition, the intercalating of K atoms into g-C₃N₄ contributes to the charge separation and transfer between adjacent layers, which is beneficial for the improved visible light photocatalytic performance [36]. Apart from K doping, halogen doped g-C₃N₄ have recently [37–42] shown promising photo-response and photocatalytic activity because of the prolong optical absorption as well as efficient

charge separation. It is noted that halogenation not only narrows the band gap but also accelerates the charge carriers transfer rate. Clearly, K or halogen doping can improve the photocatalytic activity by modulating the essential electronic band structure of g-C₃N₄, and further improving visible light harvesting and separation rate of photo-generated charge for H₂ production.

Notably, the simultaneous doping of two kinds of atoms into g-C₃N₄ such as O, S co-doping [43], P, S co-doping [44] and K, O co-doping [45] has been proved to show higher photocatalytic activity and special physicochemical characteristics in comparison with simplex element doping. For examples, O, S co-doped g-C₃N₄ (CNUS) with enhanced π-π* and n-π* electron transitions showed improved photocatalytic hydrogen production and degradation of Rhodamine B under visible-light irradiation because of the improved effects of both visible light adsorption and photogenerated carries transport [43]. In addition, O, K-functionalized g-C₃N₄ could boost the interlayer van der Waals interaction and accelerate the spatially oriented charge separation confirmed by density functional theory calculations (DFT). In such structure, the intralayer modification by O and the interlayer intercalation by K enabled the oriented charge flow both in intralayers and interlayers, which enhanced the accumulation of the localized electrons and promoted the formation of active radicals for reactants [45]. Therefore, it can be expected that simultaneous doping of two kinds of atoms is a win-win strategy to reach one plus one is greater than two results. However, developing K, halogen co-doped g-C₃N₄ materials for boosting photocatalytic activity is highly desirable, but has yet to be reported so far.

In this paper, we integrate the favorable feature of two foreign atoms doping (K and halogen doped g-C₃N₄, denoted as X-K-C₃N₄, X = F, Cl, Br, I) to investigate a superior g-C₃N₄ based photocatalyst. We for the first time report heteroatoms K, halogen binary-doped g-C₃N₄ via an ecofriendly one-step thermal polymerization method, in which a mixture of melamine and potassium halide was directly calcined in air condition. The resultant X-K-C₃N₄ exhibits improved visible light harvesting ability and photogenerated charge separation rate, resulting in enhanced photocatalytic activity. In addition, we find that F and K co-doping g-C₃N₄ can optimize the electronic-band structure which is beneficial for the reducibility of photo-driven electrons toward H₂ generation. Specially, the F-K-C₃N₄ exhibits the highest photocatalytic hydrogen evolution rate under visible-light irradiation ($\lambda \geq 420$ nm), which is nearly 8.5 times higher than the pristine one.

Results and discussion

Crystal structure of carbon nitride

The crystal structure of the g-C₃N₄ and X-K-C₃N₄ semiconductors was investigated by X-ray diffraction (XRD), Raman and Fourier transformed infrared (FTIR) spectra. As shown in Fig. 1a, all samples exhibit similar XRD patterns, suggesting the successful preparation of graphitic-like carbon nitride phase by thermally induced polymerization reaction

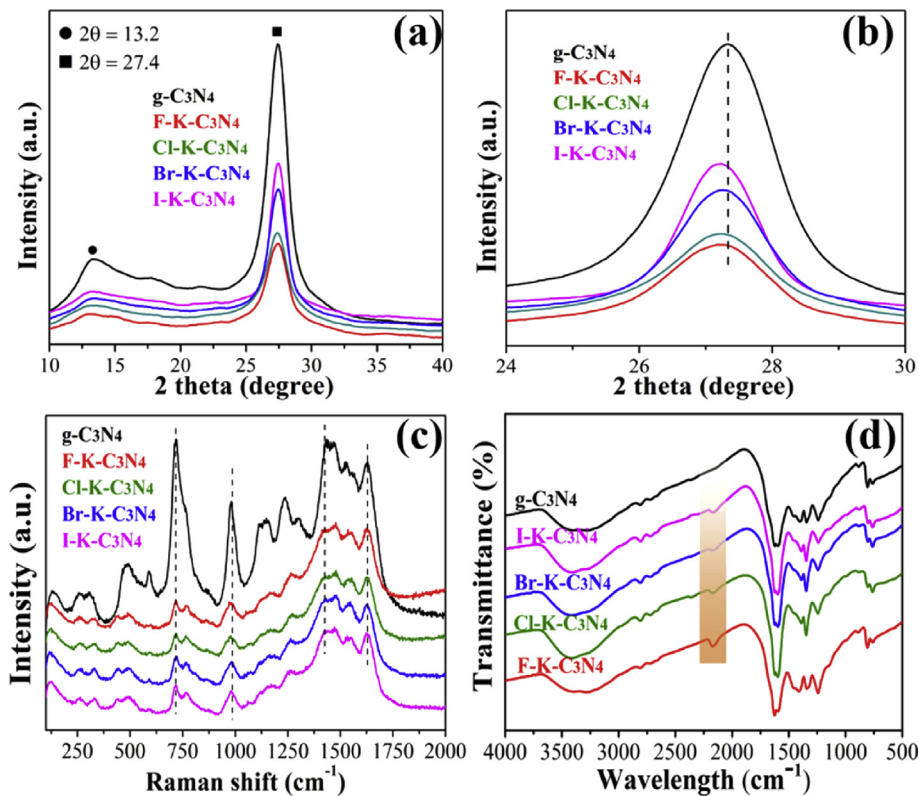


Fig. 1 – (a) XRD patterns, **(b)** the enlarged profile of the (002) diffraction region **(c)** Raman spectra (325 nm excitation) and **(d)** FT-IR spectra of $\text{g-C}_3\text{N}_4$ and $\text{X-K-C}_3\text{N}_4$.

and melamine was used as the precursor. Two distinct XRD peaks at $2\theta = 13.2^\circ$ (related to the in-plane repeating units of the heptazine heteroatom cycles) and 27.4° (the graphitic layer stacking) are observed for all the samples, which are assigned to the (100) and (002) plane of the typical graphitic layer structures [46]. The intensity of (002) signal at 27.4° gradually decreasing after heteroatoms binary modifying, which suggests that the layer stacking environment of graphitic carbon nitride is slightly changed during the K and halogen atoms co-doping process [47]. It is noted that the (002) peaks downshift to the lower angle after the K and F modifications (Fig. 1b), consistent with the expansion of interlayered structure due to the intercalation of K atoms, which is confirmed by the DFT results [45]. Interestingly, it is found that the (002) diffraction of $\text{X-K-C}_3\text{N}_4$ at around 27.4° is shifted to lower angel with the introduction of halogen atoms. In addition, a larger downshift can be observed with the increase of atomic radius of halogen atoms ($\text{F} < \text{Cl} < \text{Br} < \text{I}$). We can see from the element content of all samples in Table S1. Although the initial content of all potassium halide is the same, the mass content of I in $\text{I-K-C}_3\text{N}_4$ is only 0.01 wt%. On the other hand, the $\text{F-K-C}_3\text{N}_4$ has the highest F content (0.17 wt%). This is because the higher atomic radius of I atom hinder the dopant possible of it, which on the other side increase the dopant content of K (2.7 wt%) in $\text{I-K-C}_3\text{N}_4$ sample. As result, the highest K content of $\text{I-K-C}_3\text{N}_4$ make the highest shift of (002) plane.

The peaks at 718 cm^{-1} , 977 cm^{-1} , 1430 cm^{-1} and 1633 cm^{-1} in the Raman spectra of $\text{g-C}_3\text{N}_4$ and $\text{X-K-C}_3\text{N}_4$ are observed (Fig. 1c), which can be attributed to the melem species. The

nearly unchanged Raman spectra indicate that the chemical structures of $\text{X-K-C}_3\text{N}_4$ photocatalysts are not changed by potassium halide doping. However, the introduction of K and halogen may lead to the formation of defects and the decreasing of polymerization degree of $\text{X-K-C}_3\text{N}_4$, which can be ascribed to the lower Raman signal intensities of $\text{X-K-C}_3\text{N}_4$ [48].

To further investigate the structure of the as-prepared polymers, FT-IR spectra of all samples were analyzed. As shown in Fig. 1d, the typical C–N heterocycle stretches at $1200\text{--}1600\text{ cm}^{-1}$ and the breathing mode of the tris-triazine units at 800 cm^{-1} support the formation of extended network of C–N–C bonds in all samples. It is noted that the new peak at around 2170 cm^{-1} attributed to $\text{C}\equiv\text{N}$ triple bonds are appeared for $\text{X-K-C}_3\text{N}_4$ samples after the introduction of K and halogen. This result clearly indicates the formation of cyano-terminal $\text{C}\equiv\text{N}$ functional groups in $\text{X-K-C}_3\text{N}_4$ [40,49]. It has been deeper studied that the present of $\text{C}\equiv\text{N}$ functional groups as electron acceptors is beneficial for the photocatalytic process because of its highly efficient in charge transfer and separation [50]. Therefore, we find that the introduction of K and halogen not only leads to lower the crystallinity and simultaneous dope foreign atoms, but also importantly, results in the formation of new functional $\text{C}\equiv\text{N}$ triple bonds. Specially, the intensity of $\text{C}\equiv\text{N}$ functional groups increase with the increase of electronegativity of the halogen atom ($\text{F} > \text{Cl} > \text{Br} > \text{I}$). The lower atomic radius and higher electronegativity of F make it easier to substitute the N atoms and form new cyano-terminal $\text{C}\equiv\text{N}$ functional groups,

confirmed by the higher F content in F-K-C₃N₄ according to the results of element analysis shown in **Table S1**. The C/N ratio of F-K-C₃N₄ is 0.77, which is higher than the pristine one (0.74). This is because that the substitution of F atoms is mainly taken place in N sites and the F doping efficiency of F-K-C₃N₄ is higher. The higher F content in F-K-C₃N₄ indicates that the C–F bond is much stable than C–Br, C–Cl and C–I bond owing to the larger atomic radius of Br, Cl and I, which is similar to the previous study [51].

The morphologies of g-C₃N₄ and F-K-C₃N₄ were investigated by scanning electron microscope (SEM) and transmission electron microscope (TEM), as shown in **Fig. 2**. All the samples display a similar morphology with a stacked structure [52] (**Fig. 2a** and **d**). Taking F-K-C₃N₄ as example, the corresponding elemental mapping (**Fig. 2e**) confirm the uniform distribution of carbon, nitrogen, fluoride and potassium atoms in the whole sample. This means that our strategy can obtain homogeneous doping effect. Therefore, the introduction of K and halogen here presents little influence on the morphology and crystal structure of C₃N₄, that is, the basic 2D conjugated structure of graphitic carbon nitride is maintained, which can be confirmed by the N₂ adsorption-desorption results. The specific surface of all samples are nearly unchanged, around 10 m² g⁻¹ (**Fig. S1**, **Fig. S2** and **Table S2**).

To further analyze their chemical bonds and elemental compositions, X-K-C₃N₄ and g-C₃N₄ were tested by X-ray photoelectron spectroscopy (XPS) and the full spectrum was shown in **Fig. S3**. In **Fig. 3a**, the high resolution of N 1s spectra can be divided into three peaks with bonding energy at 398.8, 399.9 and 401.1 eV, respectively. These peaks are assigned to the sp² bonded nitrogen in triazine rings (C–N=C), the tertiary nitrogen (N–(C)₃) groups, the surface uncondensed amino groups (N–H) [41,53]. As shown in **Fig. 3b**, the C 1s peaks with binding energy values of 284.9 and 288.3 eV, corresponding to sp²-bonded carbon (N–C=N) and graphitic carbon (C–C), respectively. High-resolution spectra of N 1s and C 1s reveal that N 1s band undergoes an obvious binding-energy shift, demonstrating that their chemical environments are affected [37]. In addition, as shown in **Fig. 3c**, the F 1s peak centered at 690.1 eV demonstrates that F atoms are doped into the carbon nitride structure [54], which is reasonably considered to be originated from C–F bonds formed in F-K-C₃N₄. The chemical states of potassium are revealed by measuring K 2p levels using XPS, which exhibits two peaks at 293.0 and 295.7 eV, corresponding to K 2p_{3/2} and K 2p_{1/2}, respectively [55]. Together with these results, it can be predicted that the different structure of X-K-C₃N₄ will potential exhibit a different photoelectric behavior.

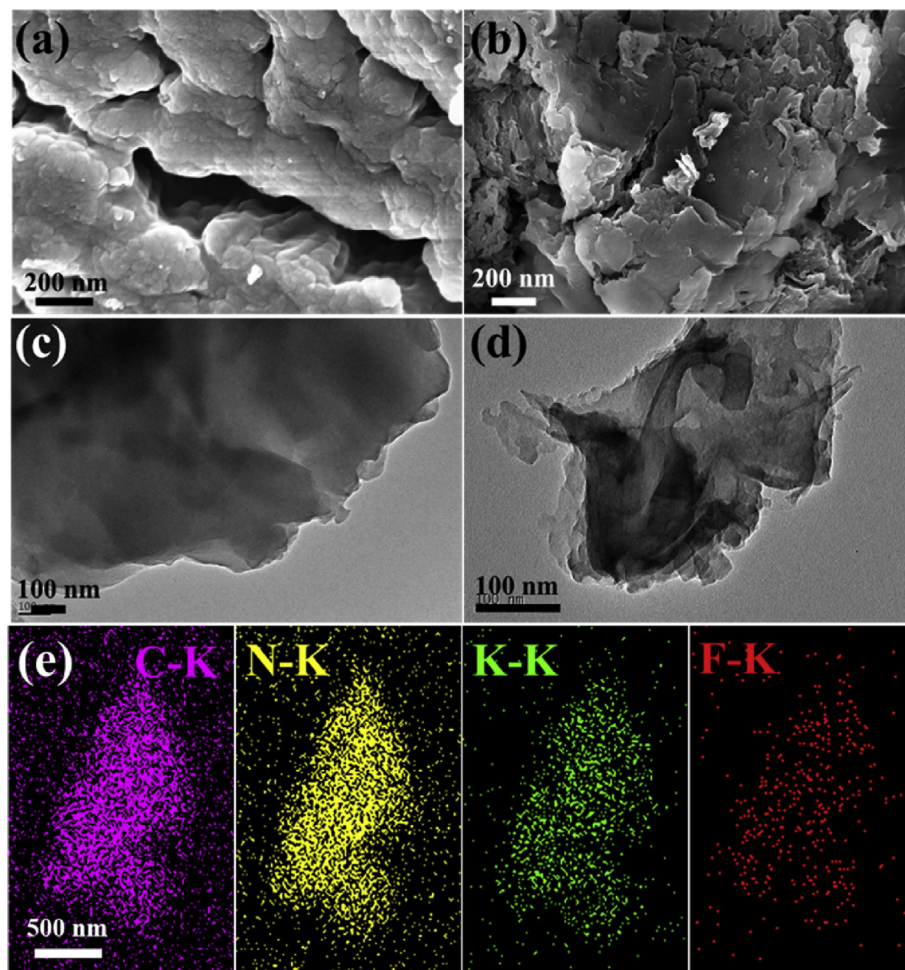


Fig. 2 – Structural characteristics of the catalysts: SEM images of (a) g-C₃N₄ and (b) F-K-C₃N₄ and TEM images of (c) g-C₃N₄ and (d) F-K-C₃N₄, (e) the EDS element mapping of F-K-C₃N₄.

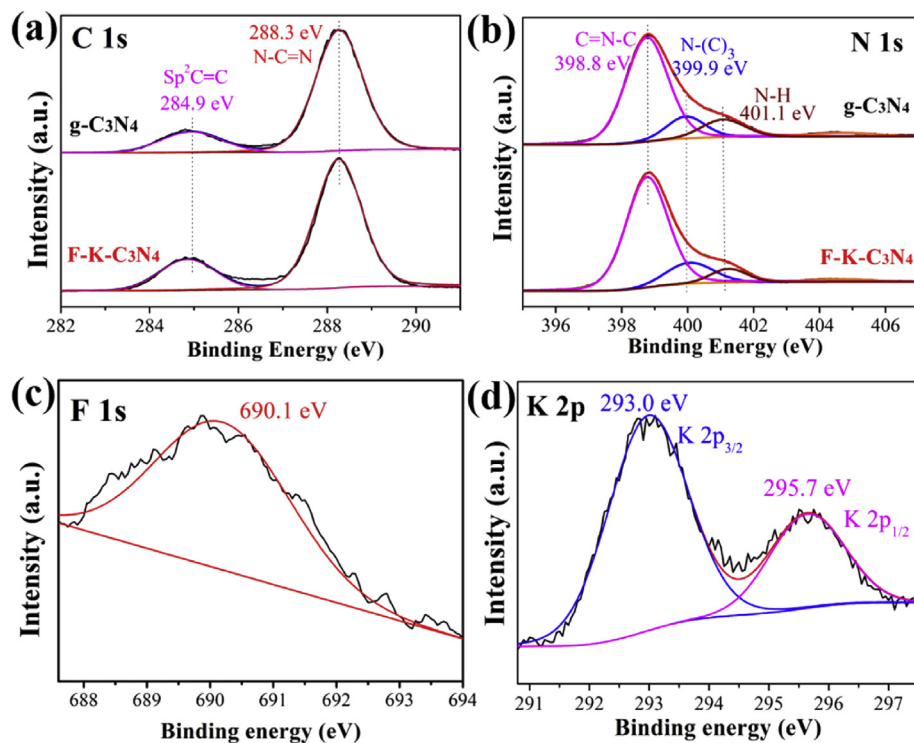


Fig. 3 – (a) C 1s and (b) N 1s XPS spectra of $\text{g-C}_3\text{N}_4$ and $\text{F}-\text{K}-\text{C}_3\text{N}_4$, (c) F 1s and (d) K 2p XPS spectra of $\text{F}-\text{K}-\text{C}_3\text{N}_4$.

Optimized photoelectrical properties

To clarify the effect of binary element doping on the photoelectrical properties of $\text{X}-\text{K}-\text{C}_3\text{N}_4$ materials, the UV-vis diffuse reflectance spectra, photoluminescence (PL) and valance band X-ray photoelectron spectroscopy (VB XPS) were carefully investigated. The UV-vis diffuse reflectance spectra results are shown in Fig. 4a. It is clearly observed that all the samples exhibit the typical semiconductor absorption. The intrinsic absorption edge of $\text{X}-\text{K}-\text{C}_3\text{N}_4$ shows a little red-shift compared with the pristine $\text{g-C}_3\text{N}_4$. The Kubelka-Munk method is used to calculate the band gap energy of all samples, as shown in Fig. 4b. It is clearly that the introduction of K and halogen atoms could narrow the bandgap structure. Specially, the band gap of $\text{X}-\text{K}-\text{C}_3\text{N}_4$ decrease from 2.71 to 2.61 eV owing to the different atomic radius of F, Cl, Br and I. It is understandable that different atomic radius presents a different extend on crystal structure and thus for different bandgap structure. According to the results of the valence band X-ray photoelectron spectroscopy (VB XPS), the positions of the valence band (VB) are estimated to be 1.85 and 1.96 eV for $\text{g-C}_3\text{N}_4$ and $\text{F}-\text{K}-\text{C}_3\text{N}_4$, respectively, as shown in Fig. 4c. Therefore, together with the studies of bandgap structure, the conducted band (CB) position can be estimated. As shown in Fig. 4d, the conduction band is -0.86 eV and -0.71 eV for $\text{g-C}_3\text{N}_4$ and $\text{F}-\text{K}-\text{C}_3\text{N}_4$, respectively.

The PL is a highly sensitive technique to further understand the transfer and recombination of photoinduced charged carriers. Fig. 4e shows the PL spectra of the five samples excited at 365 nm at room temperature. Such a band-

band PL signal is attributed to the excitonic PL, which mainly results from $n-\pi^*$ electronic transitions involving the long pairs of nitrogen atoms in $\text{g-C}_3\text{N}_4$ [47]. A sharp decrease could be observed after the introduction of binary heteroatoms into the framework, which certifies that the binary heteroatoms doping is an effective method to lower combination rate of photogenerated electron-hole pairs.

To better understand the electron transfer property, the transient photocurrent responses and electrochemical impedance spectroscopy (EIS) of $\text{g-C}_3\text{N}_4$ and $\text{X}-\text{K}-\text{C}_3\text{N}_4$ were recorded. As shown in Fig. 4f, after several on-off cycles of intermittent under visible light irradiation, the photocurrent is remarkable enhanced along with the introduction of K and halogen atoms. It is noteworthy that the photocurrent intensity displays an order of $\text{F}-\text{K}-\text{C}_3\text{N}_4 > \text{Cl}-\text{K}-\text{C}_3\text{N}_4 > \text{Br}-\text{K}-\text{C}_3\text{N}_4 > \text{I}-\text{K}-\text{C}_3\text{N}_4 > \text{g-C}_3\text{N}_4$. On the other hand, EIS Nyquist analysis is widely applied in the study of charge transfer processes on the surface of electrode. The EIS results indicate that the $\text{X}-\text{K}-\text{C}_3\text{N}_4$ shows an easier charge transfer rate (Fig. 4g) because of the changed charge distribution of $\text{g-C}_3\text{N}_4$, which is consistent with the photocurrent results. Together with above characterization, we believe that the K and halogen co-doped method is a highly efficient strategy for promoting the photoelectric properties, which is certainly favorable to enhance a better photocatalytic activity.

Photocatalytic performance

The photocatalytic performance of the as-prepared samples has been tested toward hydrogen evolution reaction (HER) by

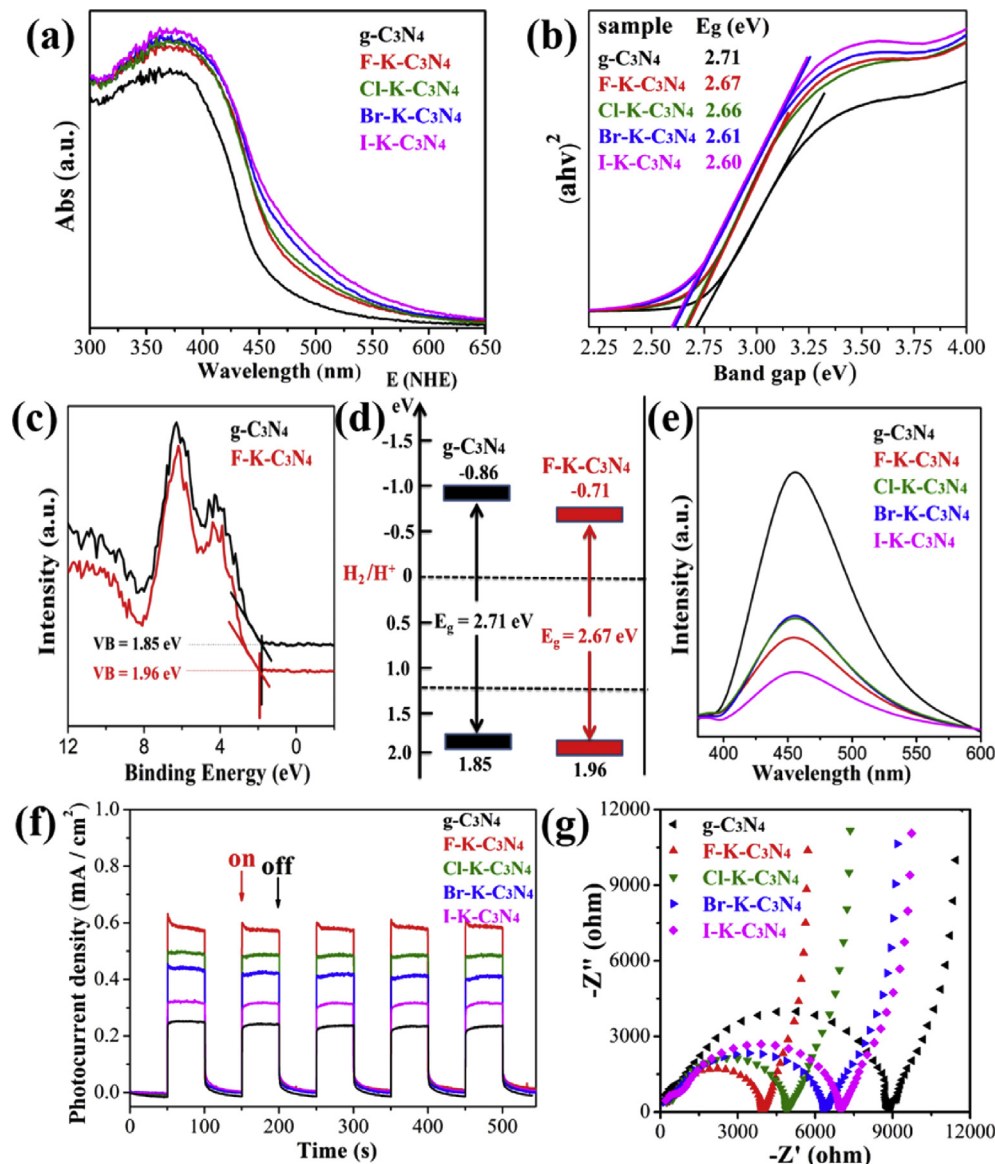


Fig. 4 – (a) UV–vis diffuse reflectance spectra and **(b)** bandgap energy for g-C₃N₄ and X-g-C₃N₄, **(c)** VB XPS spectra and **(d)** band structure diagram for g-C₃N₄ and F–K–C₃N₄, **(e)** PL spectra, **(f)** Photocurrent response under visible light irradiation and **(g)** Electrochemical impedance spectroscopy plots for g-C₃N₄ and X-K–C₃N₄.

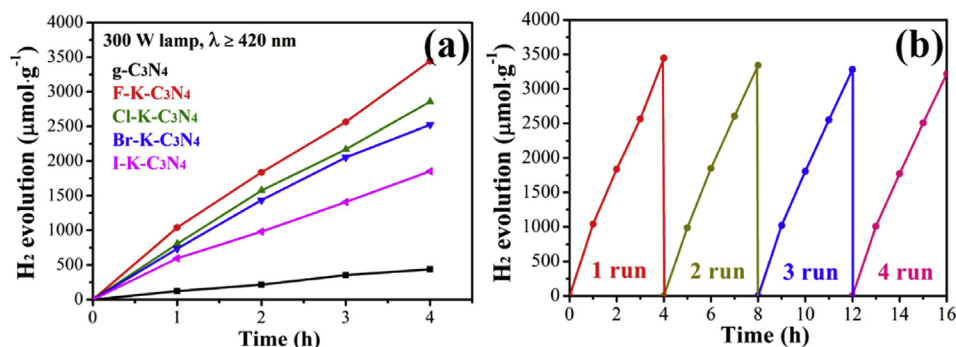


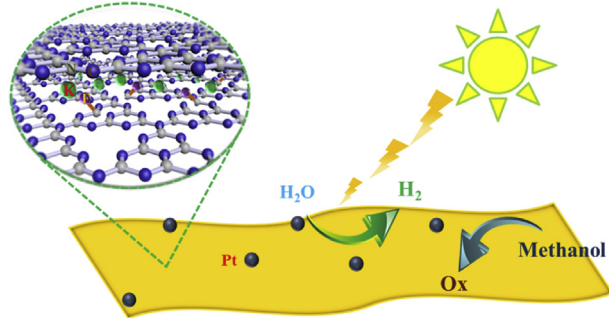
Fig. 5 – (a) H₂ generation rate over g-C₃N₄ and X-K–C₃N₄ catalysts and **(b)** Recycle of H₂ evolution of F–K–C₃N₄ photocatalyst.

evaluating the amount of H_2 from water in presence of methanol and 3 wt% of Pt under visible-light irradiation ($\lambda \geq 420$ nm). As shown in Fig. 5a, the rate of H_2 evolution on $F-K-C_3N_4$ reaches $1039 \mu\text{mol g}^{-1} \text{h}^{-1}$, which is about 8.5 times the rate of the $g-C_3N_4$ ($122 \mu\text{mol g}^{-1} \text{h}^{-1}$), which can be attributed to the highest photogenerated charge utilization efficiency after fluorine and potassium co-doping. For the simple dopant C_3N_4 , $F-C_3N_4$ and $K-C_3N_4$, the photocatalytic performance is lower than $F-K-C_3N_4$ shown in Fig. S4, indicating the double promoted effect of K and F dopants. Meanwhile, the rate is positive correlated with electronegativity of halogen elements in potassium halide. The photocatalytic performance is highly related to the separation rates of photogenerated electrons and holes, which is determined by the efficient K and F dopants. The different activity of $X-K-C_3N_4$ caused by distinct doping efficiency of halogen atoms, as confirmed by the different element composition (Table S1). The reduced atomic radius and increased electronegativity of the F element result in higher doping efficiency of $F-K-C_3N_4$, which generates more defected active sites for the separation of carriers thereby enhanced the photocatalytic performance. The catalytic stability of H_2 evolution on $F-K-C_3N_4$ is evaluated by four cycling tests (16 h) under the same conditions, as shown in Fig. 5b. The amount of H_2 production keeps constant without noticeable deactivation after four cycles, which confirms that $F-K-C_3N_4$ photocatalyst is stable during the photocatalytic H_2 evolution. This is because the heteroatoms intercalated into the π -conjugated system of $g-C_3N_4$ can accelerate the transport of photogenerated electrons and restrain the recombination of carriers, which could improve the photocatalytic activity.

Discussion

There are two main reasons can be concluded as vital features for the enhanced photo-activity of $F-K-C_3N_4$. Firstly, the unique structure of $F-K-C_3N_4$ enhances the light absorption. Second, The K and F co-doping structure of $F-K-C_3N_4$ expedites the lifetime and decrease the recombination of photo-induced electron-hole both in intralayers and interlayers.

Firstly, UV-vis absorption spectra show that $g-C_3N_4$ barely absorbed the visible light while $F-K-C_3N_4$ has a wide adsorption of visible light. The narrow bandgaps of $F-K-C_3N_4$ (2.67 eV) promotes the availability of the visible light and increases the charge carrier separation rate. This indicate that the fluorine and potassium co-doping can modify the band structure configuration of $F-K-C_3N_4$, which can activate the photon absorption process (the initial step of photocatalysis) and finally improve photocatalytic performance. In addition, the mid-gap states created by the F impurity in intralayers makes the band gap slightly narrower and results in enhanced optical absorption, which confirmed by the existence of C–F bond in XPS result and the higher C/N ratio in element analysis. Importantly, the C≡N triple bond plays an important part for the transformation of photogenerated carriers on the intralayers. Together, the existence of C–F and C≡N bond accelerate transition of photoinduced electrons on the intralayers simultaneously. On the other hand, the impurity can serve as the electron or hole traps contributed to suppressing



Scheme 1 – Photocatalytic H_2 production mechanism of 3 wt% Pt/ $F-K-C_3N_4$ photocatalyst.

the recombination of photogenerated charge carriers, which is essential to improve the photocatalytic performance. In such way, the charge recombination is effectively suppressed and superior photoreduction performance is achieved.

Secondly, the intercalating alkali metals between interlayers can create an internal electric field (IEF) [45,56]. IEF is additional factor for further accelerate the separation of electrons in our case similarly. The mediated interlayered electrons channel by K doing supplys additional impetus for charge separation between interlayers and the directional electrons can expeditiously transfer crossing multiple layers. This effect makes the photogenerated electrons easier reach the catalyst's surface to participate photocatalytic process. In comparison with pristine C_3N_4 , the lifetime of photogenerated charge carriers in $F-K-C_3N_4$ is prolonged, confirming that the formation of IEF effectively boosts the charge separation and transfer. These photoelectrical properties demonstrate that the $F-K-C_3N_4$ is efficient in suppressing charge carrier recombination, and as a result, they can reach an excellent catalytic activity, confirmed by the studies of PL, photocurrent density and EIS.

Therefore, the enhanced visible light absorption, faster carriers' transmission and the existence of IEF coming from the K, F co-functional structure are believed to lead to increase in the photocatalytic H_2 evolution activity. According to above analysis, a possible mechanism for the photocatalytic activity on $F-K-C_3N_4$ is proposed and schematically illustrated in Scheme 1. In short, C–F bond and C≡N bond, and K bridge facilitate the carriers transmission in intralayers and interlayers, respectively, which is important for the utilization of photodriven electrons, and result in an enhanced photocatalytic performance.

Conclusion

In summary, we successfully prepared $X-K-C_3N_4$ by a simply thermal polymerization and the structure, surface, morphology and element chemical states were investigated and discussed in detail. $F-K-C_3N_4$ shows outstanding photocatalytic performance for hydrogen production from water under visible light irradiation. The significantly enhanced photocatalytic activity is described to the higher doping rate of F[−] ion caused by low atomic radius and high C–F bonds

stability. In addition, the K, F binary doping could bring the C≡N triple bond into the X-K-C₃N₄ structure, which is very important for the transformation of photoinduced electrons. The introduction of heteroatoms not only inhibits photoelectron-hole recombination probability but also alter the bandgap configuration of X-K-C₃N₄. Such modifications in intrinsic electronic structure and band positions consequently can improve the photocatalytic activity of X-K-C₃N₄. The double accelerations of F, K binary doping in the electron's transmission in both intralayers and interlayers related to the photocatalytic performance are systematically described. More importantly, the F-K-C₃N₄ shows great potential in the application of other solar energy conversion.

Acknowledgements

This work is supported by the National Natural Science Foundation of China (No. 21773195), the Fundamental Research Funds for the Central Universities (No. 20720170030).

Appendix A. Supplementary data

Supplementary data to this article can be found online at <https://doi.org/10.1016/j.ijhydene.2019.09.013>.

REFERENCES

- [1] Chen X, Shen S, Guo L, Mao SS. Semiconductor-based photocatalytic hydrogen generation. *Chem Rev* 2010;110:6503–70.
- [2] Han C, Wu L, Lei G, Li Y, Zhen Z. AuPd bimetallic nanoparticles decorated graphitic carbon nitride for highly efficient reduction of water to H₂ under visible light irradiation. *Carbon* 2015;92:31–40.
- [3] Cihlar J, Kasperek V, Kralova M, Castkova K. Biphasic anatase-brookite nanoparticles prepared by sol-gel complex synthesis and their photocatalytic activity in hydrogen production. *Int J Hydrogen Energy* 2015;40:2950–62.
- [4] Devi Suman, Korake Prakash, Achary SN, et al. Genesis of enhanced photoactivity of CdS/Nix nanocomposites for visible-light-driven splitting of water. *Int J Hydrogen Energy* 2014;39:19424–33.
- [5] Fujishima A, Honda K. Electrochemical photolysis of water at a semiconductor electrode. *Nature* 1972;238:37.
- [6] Chen X, Chen H, Guan J, Zhen J, Sun Z, Du P, et al. A facile mechanochemical route to a covalently bonded graphitic carbon nitride (g-C₃N₄) and fullerene hybrid toward enhanced visible light photocatalytic hydrogen production. *Nanoscale* 2017;9:5615–23.
- [7] Liu G, Niu P, Sun C, Smith SC, Chen Z, Lu GQ, et al. Unique electronic structure induced high photoreactivity of sulfur-doped graphitic C₃N₄. *J Am Chem Soc* 2010;132:11642–8.
- [8] Yao W, Huang C, Muradov N, T-Raissi A. A novel Pd-Cr₂O₃/CdS photocatalyst for solar hydrogen production using a regenerable sacrificial donor. *Int J Hydrogen Energy* 2011;36:4710–5.
- [9] Bi J, Fang W, Li L, Wang J, Liang S, He Y, et al. Covalent triazine-based frameworks as visible light photocatalysts for the splitting of water. *Macromol Rapid Commun* 2015;36:1799–805.
- [10] Jiang Q, Li L, Bi J, Liang S, Liu M. Design and synthesis of TiO₂ hollow spheres with spatially separated dual cocatalysts for efficient photocatalytic hydrogen production. *Nanomaterials* 2017;7:24.
- [11] Melián EP, Díaz OG, Méndez AO, López CR, Suárez MN, Rodríguez JMD, et al. Efficient and affordable hydrogen production by water photo-splitting using TiO₂-based photocatalysts. *Int J Hydrogen Energy* 2013;38:2144–55.
- [12] Tian M, Wang H, Sun D, Peng W, Tao W. Visible light driven nanocrystal anatase TiO₂ doped by Ce from sol-gel method and its photoelectrochemical water splitting properties. *Int J Hydrogen Energy* 2014;39:13448–53.
- [13] Bao P, Yu W, Liang Y, Luo S, Su W, Wang X. Nanocomposite of BiPO₄ and reduced graphene oxide as an efficient photocatalyst for hydrogen evolution. *Int J Hydrogen Energy* 2014;39:13527–33.
- [14] Zhang J, Wang B, Wang X. Carbon nitride polymeric semiconductor for photocatalysis. *Prog Chem* 2014;26:19–29.
- [15] Tian Y, Ge L, Wang K, Chai Y. Synthesis of novel MoS₂/g-C₃N₄ heterojunction photocatalysts with enhanced hydrogen evolution activity. *Mater Char* 2014;87:70–3.
- [16] Wang B, Li C, Hirabayashi D, Suzuki K. Hydrogen evolution by photocatalytic decomposition of water under ultraviolet-visible irradiation over K₂La₂Ti_{3-x}M_xO_{10+delta} perovskite. *Int J Hydrogen Energy* 2010;35:3306–12.
- [17] Cheng Z, Zheng K, Lin G, Fang S, Li L, Bi J, et al. Constructing a novel family of halogen doped covalent triazine-based frameworks as efficient metal-free photocatalysts for hydrogen production. *Nanoscale Adv* 2019;1:2674–80.
- [18] Tay Q, Kanhere P, Ng CF, Chen S, Chakraborty S, Huan ACH, et al. Defect engineered g-C₃N₄ for efficient visible light photocatalytic hydrogen production. *Chem Mater* 2015;27:4930–3.
- [19] Wang X, Maeda K, Thomas A, Takanabe K, Xin G, Carlsson JM, et al. A metal-free polymeric photocatalyst for hydrogen production from water under visible light. *Nat Mater* 2008;8:76–80.
- [20] Zhang J, Chen X, Takanabe K, Maeda K, Domen K, Epping JD, et al. Synthesis of a carbon nitride structure for visible-light catalysis by copolymerization. *Angew Chem* 2010;49:441–4.
- [21] Fresno F, Portela R, Suarez S, Coronado J. Photocatalytic materials: recent achievements and near future trends. *J Mater Chem* 2014;2:2863–84.
- [22] Cao S, Yu J. g-C₃N₄-Based photocatalysts for hydrogen generation. *J Phys Chem Lett* 2013;4:2101–7.
- [23] Fajrina N, Tahir M. A critical review in strategies to improve photocatalytic water splitting towards hydrogen production. *Int J Hydrogen Energy* 2019;44:540–77.
- [24] Chen D, Wang K, Hong W, Zong R, Yao W, Zhu Y. Visible light photoactivity enhancement via CuTCPP hybridized g-C₃N₄ nanocomposite. *Appl Catal B Environ* 2015;166–167:366–73.
- [25] Li XH, Antonetti M. ChemInform Abstract: metal nanoparticles at mesoporous N-doped carbons and carbon nitrides: functional mott-Schottky heterojunctios for catalysis. *Chem Soc Rev* 2013;42:6593–604.
- [26] Yan SC, Li ZS, Zou ZG. Photodegradation of rhodamine B and methyl orange over boron-doped g-C₃N₄ under visible light irradiation. *Langmuir the Acs J Surface Colloids* 2010;26:3894–901.
- [27] Lan DH, Wang HT, Chen L, Au CT, Yin SF. Phosphorous-modified bulk graphitic carbon nitride: facile preparation and application as an acid-base bifunctional and efficient

- catalyst for CO₂ cycloaddition with epoxides. *Carbon* 2016;100:81–9.
- [28] Wang X, Zhang G, Lan ZA, Lin L, Lin S. Overall water splitting by Pt/g-C₃N₄ photocatalysts without using sacrificial agent. *Chem Sci* 2016;7:3062–6.
- [29] Zhu M, Kim S, Mao L, Fujitsuka M, Zhang J, Wang X, et al. Metal-Free photocatalyst for H₂ evolution in visible to near-infrared region: black phosphorus/graphitic carbon nitride. *J Am Chem Soc* 2017;139:13234–42.
- [30] Ge L, Han C, Liu J. Novel visible light-induced g-C₃N₄/Bi₂WO₆ composite photocatalysts for efficient degradation of methyl orange. *Appl Catal B Environ* 2011;108:100–7.
- [31] Yan H, Huang Y. Polymer composites of carbon nitride and poly(3-hexylthiophene) to achieve enhanced hydrogen production from water under visible light. *Chem Commun* 2011;47:4168–70.
- [32] Chen X, Zhang J, Fu X, Antonietti M, Wang X. Fe-g-C₃N₄-catalyzed oxidation of benzene to phenol using hydrogen peroxide and visible light. *J Am Chem Soc* 2009;131:11658–9.
- [33] Kamegawa T, Matsuura S, Seto H, Yamashita H. A visible-light-harvesting assembly with a sulfocalixarene linker between dyes and a Pt-TiO₂ photocatalyst. *Angew Chem* 2013;52:916–9.
- [34] Liu Q, Shen J, Yu X, Yang X, Xu J. Unveiling the origin of boosted photocatalytic hydrogen evolution in simultaneously (S, P, O)-codoped and exfoliated ultrathin g-C₃N₄ nanosheets. *Appl Catal B Environ* 2019;248:84–94.
- [35] Li J, Shen B, Hong Z, Lin B, Gao B, Chen Y. A facile approach to synthesize novel oxygen-doped g-C₃N₄ with superior visible-light photoreactivity. *Chem Commun* 2012;48:12017–9.
- [36] Xiong T, Cen W, Zhang Y, Dong F. Bridging the g-C₃N₄ interlayers for enhanced photocatalysis. *ACS Catal* 2016;6:2462–72.
- [37] Liu C, Zhang Y, Dong F, Reshak AH, Ye L, Pinna N, et al. Chlorine intercalation in graphitic carbon nitride for efficient photocatalysis. *Appl Catal B Environ* 2017;203:465–74.
- [38] Ong WJ, Tan LL, Ng YH, Yong ST, Chai SP. Graphitic carbon nitride (g-C₃N₄)-based photocatalysts for artificial photosynthesis and environmental remediation: are we a step closer to achieving Sustainability. *Chem Rev* 2016;116:7159–329.
- [39] Ma F, Sun C, Shao Y, Wu YZ, Huang B, Hao X. One-step exfoliation and fluorination of g-C₃N₄ nanosheets with enhanced photocatalytic activities. *New J Chem* 2017;41:3061–7.
- [40] Wang Y, Di Y, Antonietti M, Li H, Chen X, Wang X. Excellent visible-light photocatalysis of fluorinated polymeric carbon nitride solids. *Chem Mater* 2010;22:5119–21.
- [41] Lan ZA, Zhang G, Wang X. A facile synthesis of Br-modified g-C₃N₄ semiconductors for photoredox water splitting. *Appl Catal B Environ* 2016;192:116–25.
- [42] Jiang B, Huang Y, Yan Q, Yan H, Tang Y, Chen S, et al. Layer stacking-like iodine and phosphorus Co-doped C₃N₄ for enhanced visible-light photocatalytic hydrogen evolution. *ChemCatChem* 2017;9:4083–6.
- [43] Chen Z, Fan T, Shao M, Yu X, Wu Q, Li J, et al. Simultaneously enhanced photon absorption and charge transport on a distorted graphitic carbon nitride toward visible light photocatalytic activity. *Appl Catal B Environ* 2019;242:40–50.
- [44] Jiang L, Yuan X, Zeng G, Chen X, Wu Z, Liang J, et al. Phosphorus-and sulfur-codoped g-C₃N₄: facile preparation, mechanism insight, and application as efficient photocatalyst for tetracycline and methyl orange degradation under visible light irradiation. *ACS Sustainable Chem Eng* 2017;5:5831–41.
- [45] Li J, Zhang Z, Cui W, Wang H, Cen W, Johnson G, et al. The spatially oriented charge flow and photocatalysis mechanism on internal van der Waals heterostructures enhanced g-C₃N₄. *ACS Catal* 2018;8:8376–85.
- [46] Bojdys MJ, Müller JO, Antonietti M, Thomas A. Ionothermal synthesis of crystalline, condensed, graphitic carbon nitride. *Chemistry-A Eur J* 2008;14:8177–82.
- [47] Hu S, Li F, Fan Z, Wang F, Zhao Y, Lv Z. Band gap-tunable potassium doped graphitic carbon nitride with enhanced mineralization ability. *Dalton Trans* 2014;44:1084–92.
- [48] Jürgens B, Irran E, Senker J, Kroll P, Müller H, Schnick W. Melem (2,5,8-triamino-tri-s-triazine), an important intermediate during condensation of melamine rings to graphitic carbon nitride: synthesis, structure determination by X-ray powder diffractometry, solid-state NMR, and theoretical studies. *J Am Chem Soc* 2003;125:10288.
- [49] Gao H, Yan S, Wang J, Huang YA, Wang P, Li Z, et al. Towards efficient solar hydrogen production by intercalated carbon nitride photocatalyst. *Phys Chem Chem Phys – PCCP* 2013;15:18077–84.
- [50] Liu G, Zhao G, Zhou W, Liu Y, Pang H, Zhang H, et al. In situ bond modulation of graphitic carbon nitride to construct p–n homojunctions for enhanced photocatalytic hydrogen production. *Adv Funct Mater* 2016;26:6822–9.
- [51] O'Hagan D. Understanding organofluorine chemistry. An introduction to the C-F bond. *Chem Soc Rev* 2008;37:308–19.
- [52] Bojdys MJ, Mäller JO, Antonietti M, Thomas A. Ionothermal synthesis of crystalline, condensed, graphitic carbon nitride. *Chemistry* 2008;14:8177–82.
- [53] Liu J, Zhang T, Wang Z, Dawson G, Chen W. Simple pyrolysis of urea into graphitic carbon nitride with recyclable adsorption and photocatalytic activity. *J Mater Chem* 2011;21:14398–401.
- [54] Palchan I, Crespin M, Estrade-Szwarckopf H, Rousseau B. Graphite fluorides: an XPS study of a new type of C-F bonding. *Chem Phys Lett* 1989;157:321–7.
- [55] Mo Z, Bai X, Di L, Wang J, Zhu Y. Enhanced catalytic activity of potassium-doped graphitic carbon nitride induced by lower valence position. *Appl Catal B Environ* 2015;164:77–81.
- [56] Wang C, Qin J, Shen X, Riedel R, Harms K, Meggers E. Asymmetric radical-radical cross-coupling through visible-light-activated iridium catalysis. *Angew Chem Int Ed* 2016;55:685–8.